Atmospheric Environment 61 (2012) 180–188

Contents lists available at SciVerse ScienceDirect

Atmospheric Environment

journal homepage: www.elsevier.com/locate/atmosenv

Columnar aerosol properties in a Northeastern Atlantic site (Plymouth, United Kingdom) by means of ground based skyradiometer data during years 2000–2008

Víctor Estellés [a,b,*], Timothy J. Smyth [a], Monica Campanelli [c]

[a] Plymouth Marine Laboratory, Plymouth, United Kingdom
[b] Universitat de València, Burjassot, Valencia, Spain
[c] Istituto di Scienze dell'Atmosfera e del Clima, Rome, Tor Vergata, Italy

HIGHLIGHTS

- An 8 year aerosol climatology is presented for a northeastern Atlantic site.
- A new calibration and processing software has been used.
- The region is characterized by low aerosol optical depth and low variability.
- The aerosol properties have been classified in terms of the air mass types.
- The main aerosol is a mixture dominated by maritime particles with low concentration.

ARTICLE INFO

Article history:
Received 10 December 2011
Received in revised form
9 July 2012
Accepted 10 July 2012

Keywords:
Marine aerosols
AOD
Prede POM
ESR
SKYNET
Skyradiometer

ABSTRACT

Between 2000 and 2008, columnar optical and radiative properties were measured at the Plymouth Marine Laboratory (PML), UK (50° 21.95′N, 4° 8.85′W) using an automatic Prede POM01L sun–sky photometer. The database was analyzed for aerosol optical properties using the SKYRAD radiative inversion algorithm and calibrated using the in situ SKYIL calibration method. Retrievals include aerosol optical depth, Ångström wavelength exponent, aerosol volume distribution, refractive index and single scattering albedo. The results show that the Plymouth site is characterized by low values of aerosol optical depth with low variability (0.18 ± 0.08 at 500 nm) and a mean annual Ångström exponent of 1.03 ± 0.21. The annual mean of the single scattering albedo is 0.97, indicative of non-absorbing aerosols. The aerosol properties were classified in terms of air mass back trajectories: the area is mainly affected by Atlantic air masses and the dominant aerosol type is a mixture of maritime particles, present in low burdens with variable size. The maritime air masses were defined by annual mean values for the AOD (at 500 nm) of 0.13–0.14 and a wavelength exponent of 0.96–1.03. Episodic anthropogenic and mineral dust intrusions occasionally occur, but they are sporadic and dilute (AOD at 500 nm about 0.20). Tropical continental air masses were characterized by the highest AOD at 500 nm (0.34) and the lowest wavelength exponent (0.83), although they were the least represented in the analysis.

1. Introduction

Atmospheric aerosols play an important role in the Earth's radiation budget and therefore on the climate system (Haywood and Schulz, 2007; Intergovernmental Panel on Climate Change (IPCC), 2007). Aerosols scatter and absorb incoming solar radiation thus affecting the radiative transfer in the atmosphere. They can also act as condensation nuclei (Cruz and Pandis, 1997) modifying the microphysical and radiative characteristics of clouds. These effects are strongly dependent on the physical and radiative properties of the aerosols; therefore it is important to increase our knowledge of their global distribution and inherent properties by continuous monitoring and characterization.

Aerosol observations from international networks (such as AERONET (Holben et al., 1998), SKYNET (Takamura et al., 2004) and ESR (Campanelli et al., 2012; Estellés et al., 2012)) located in marine or coastal environments may be more important than continental

* Corresponding author. Dept. Física de la Terra I Termodinàmica, Facultat de Física, C/Dr. Moliner 50, 46100 Burjassot, Valencia, Spain. Tel.: +34 96 354 3255.
E-mail address: vestelle@uv.es (V. Estellés).

1352-2310/$ – see front matter © 2012 Elsevier Ltd. All rights reserved.
http://dx.doi.org/10.1016/j.atmosenv.2012.07.024

sites as the direct effect of aerosols on the global mean land temperature could take place through their effect on the global sea surface temperature (Hoerling et al., 2008). Therefore the Atlantic Ocean could be especially important (Zhang et al., 2007) and an aerosol climatology of the European Atlantic shores useful for parameterising climate models, especially when ship borne data is unavailable (Smirnov et al., 2011). Sun photometric data from the Northern Atlantic coastal environment are scarce: AERONET sites in the region have shorter combined databases, and tend to be plagued by clouds in the northernmost stations, reducing the amount of useful data.

This paper presents an eight year sun photometric database retrieved at the Plymouth Marine Laboratory (50° 21.95′N, 4° 8.85′W) an ESR site situated in the western English Channel (http://www.westernchannelobservatory.org.uk). The sun photometric data has been processed for a range of aerosol optical properties and the focus of this study is their temporal variability within the context of an aerosol climatology.

2. Measurement site and instrumentation

In May 2000 a Prede POM01L radiometer was deployed on the roof of PML (50° 21.95′N, 4° 8.85′W, 30 m above sea level). The PML building is located only 250 m away from the Plymouth Sound shoreline, south of the city of Plymouth (pop. 250,000). Local sources of anthropogenic pollution are the low traffic and port activities. Remote sources of anthropogenic pollution could be attributed to continental Europe and occasionally from other UK urban areas, but these are generally located downwind of the prevailing wind direction. Main sources of local natural aerosols are expected to be the Atlantic Ocean (marine aerosols) and the surrounding countryside (rural aerosols).

The POM01L is an automatic sun–sky radiometer designed for the autonomous measurement of direct solar and diffuse sky radiance. The optical head is equipped with a set of interferential filters whose transmission function is nominally centered at wavelengths 315, 400, 500, 675, 870, 936 and 1020 nm. The full width at half maximum (FWHM) is about 10 nm for the visible band channels. The diffuse sky radiance is not measured with the 315 and 936 nm channels. The optical head is also equipped with a 0.6° field of view (FOV). Such a small FOV requires an accurate sun pointing and tracking system: this is based on a four diode compensation electronic design. This pointing system is allocated in a parallel tube and it is attached to the optical head altogether with the main collimator, allowing easy adjustment.

The Prede POM radiometer is the standard instrument used in the SKYNET network in Asia (Takamura et al., 2004) and one of the standard instruments in the European Skynet Radiometers network (ESR) (Estellés et al., 2012).

Due to its continuous environmental exposure, the radiometer detector, filters and electronics are progressively degraded, causing a temporal drift of the calibration coefficients. Given that sun–sky photometers measure in two different configurations – direct solar and diffuse sky radiation – they require two types of calibration.

2.1. Solar calibration

In the SKYNET and ESR networks, the calibration of the POM radiometers is performed by applying the Skyrad Improved Langley Plot technique (Campanelli et al., 2004, 2007). Campanelli et al. (2004) estimated the calibration uncertainties using the improved method to range between 1.0% for 400 nm and 2.5% for 1020 nm. These values are very similar to that from AERONET for field instruments (Holben et al., 1998), stated to be 1.0–2.0%, which undergo a rigorous annual laboratory calibration regime.

From the resultant SKYIL calibration factors, monthly calibration averages were computed. Monthly averages were calculated if more than three values were available. These monthly mean values were fitted with lines, after visually identifying changes in trends or non linearity in their temporal evolution. Ten different calibrations sets were identified in this way. Estimated uncertainties of 1.8, 2.0, 2.2, 1.9 and 2.2% (at 400, 500, 675, 870 and 1020 respectively) were found for the definitive calibration ensemble. These spectral uncertainties were estimated as the root mean square deviation between all the fitted points and the correspondent fitted lines, and expressed in terms of the extraterrestrial constant for the instrument. The mean annual relative drift was estimated to be −3.0, −2.8, −1.7, −1.1 and −1.7%, for the period from 2001 to 2006 (at 400, 500, 675, 870 and 1020 respectively).

Fig. 1 shows the calibration series for the 500 nm channel. The linear fittings to the mean monthly values are interpolated in order to extract the correspondent values on the 15th of every month. These are the actual calibration values used in the inversion code (corrected by the Sun–Earth distance factor) and can also be visually compared here with the original data points.

In the upper plot of Fig. 1 there is a smooth decay between 2001 and 2002. The linear regression is a good approximation of the filter degradation. However, in the bottom graph, a very different scenario is represented. A sudden drop in mid-May 2004 was not recovered until mid July 2004. Both solar calibration and solid view angle (SVA or $\Delta\Omega$) values suffered a sensitivity change.

This ability to spot sudden changes of calibration values (and therefore instrumental problems) is one of the main advantages of the SKYIL in situ calibration method. Although a linear decay is usually a good (and robust) hypothesis, it occasionally fails; an enhanced in situ calibration method is a good solution for tracking non-linear drift trends, while maintaining a rather low uncertainty (1.0–2.5%) similar to that of AERONET field instruments (1.0–2.0%) and much lower than the standard Langley plot, that could reach a variation of 10% when performed at sea level (Shaw, 1976).

In Table 1 the ten different calibration series have been detailed for wavelength 500 nm. Pre- and post-calibrations and correspondent starting and ending dates are given. The estimated monthly calibration drift is also included. The average absolute monthly drift is ±0.4%/month, and it is very dependent on the state of the lenses and the pointing system.

Moreover, in Table 1 calibration factors for series 8 and 9 are not given due to problems with the optical head electronics. Although some data from these series could be still inverted, no good quality calibrations were available so the whole data series have been dismissed. Furthermore, only one calibration set has been employed for series 7. It looks reasonable to assume the same calibration for the whole series, as it was only 1.5 month long.

2.2. Diffuse sky calibration

Accurate calibration of the diffuse component in a sky–sun radiometer requires comparison with a known and traceable radiation source. For example, AERONET uses a 2 m diameter integrating sphere with 12 lamps that allow different levels of radiant intensity with an uncertainty of about 5.5% (Holben et al., 1998). However the cost of this type of calibration system is very high and usually independent research groups make use of small calibration sources with a single lamp. The related uncertainty is obviously higher in the latter case.

The Prede instrument uses another principle for the calibration of the diffuse radiance: this is done by determining it spectral solid view angle (SVA). This should be performed periodically for optimum performance of the instrument. The SVA is mainly determined by the geometry of the collimator tube and the optical head.

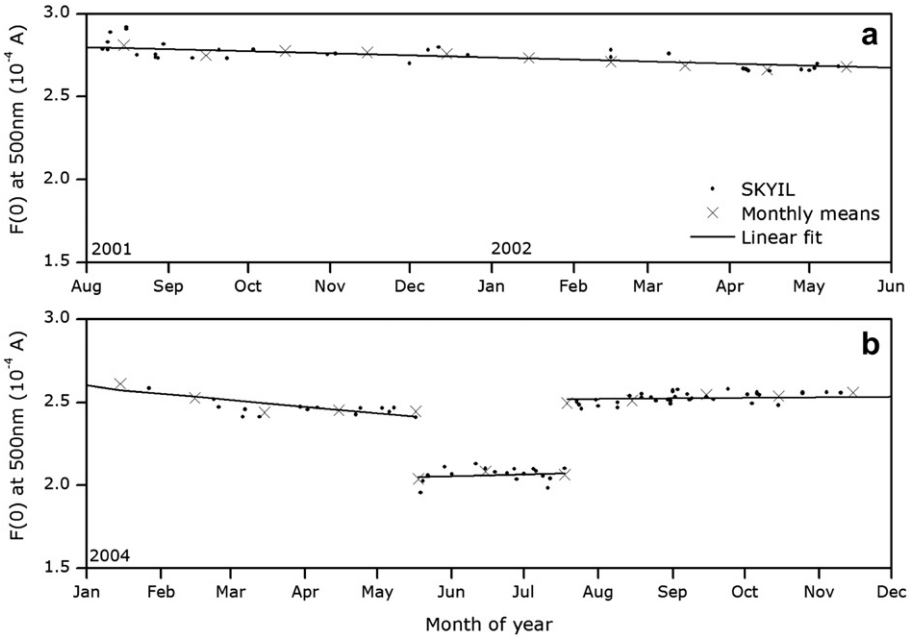

Fig. 1. Evolution of calibration factor at 500 nm for two different temporal cases: a) smooth linear decay in years 2001–2002, b) a temporal jump due to an electronic failure.

However, other factors (such as optical train misalignment or diffraction and color aberrations from the lenses, for example) affect the SVA values. The estimation of the SVA values can be performed by a spatial scanning of the clear sky solar disk which provides better stability and collimation than any laboratory source. This procedure has the added advantage of being applicable in situ (Boi et al., 1999).

3. Methodology

3.1. Radiance inversions

This work uses the SKYRAD algorithm version 4.2 for the retrieval of optical and radiative aerosol properties. Previous SKYRAD versions are described by Nakajima et al. (1983, 1996). Extensions in version 4.2 include the retrieval of aerosol refractive index.

The SKYRAD algorithm retrieves the aerosol size distribution, phase function and single scattering albedo, when the ratio between sky diffuse and sun direct signals is inverted (instead of the radiometric diffuse radiance). At ground level, the direct and diffuse components are given by:

$$F(\lambda) = F_0(\lambda)\exp[-m_0\delta(\lambda)] \quad (1)$$

$$E(\Theta) = Fm_0[\omega\delta P(\Theta) + q(\Theta)] \quad (2)$$

Table 1
Series used for the calibration factor F_0 at 500 nm. The pre (F_{0i}) and post (F_{0f}) calibrations are given at the correspondent starting and final dates of each series. The estimated monthly drift is also given. See the text for further explanations.

#	Starting date	F_{0i} (10^{-4} mA)	Final date	F_{0f} (10^{-4} mA)	Drift (%/month)
1	15/05/2001	2.226	26/07/2001	2.252	+0.43
2	27/07/2001	2.801	25/06/2002	2.666	−0.55
3	26/06/2002	2.747	16/03/2003	2.763	−0.07
4	17/03/2003	2.594	17/05/2004	2.414	−0.51
5	18/05/2004	2.051	18/07/2004	2.074	+0.56
6	19/07/2004	2.522	06/04/2006	2.348	−0.65
7	07/08/2006	2.753	19/09/2006	2.753	–
8	16/03/2007	–	27/04/2007	–	–
9	28/04/2007	–	06/06/2007	–	–
10	07/06/2007	2.762	15/03/2008	2.715	−0.20

In these equations, F is the spectral direct sun irradiance (W m^{-2} μm^{-1}) and E is the spectral diffuse sky radiance (W m^{-2} μm^{-1} Ω^{-1}). $P(\Theta)$ and ω are the total phase function and single scattering albedo respectively. Equation (1) is the Beer–Lambert equation relating the ground level measurement of direct irradiance to the extraterrestrial value F_0. F_0 is also the calibration factor in terms of irradiance after being corrected for the Sun–Earth distance. The total optical depth is given by $\delta(\lambda)$ and the optical air mass by m_0.

Equation (2) relates the diffuse sky radiance to the total phase function of the molecular and particulate ensemble that describes the angular dependence of the scattered radiation, in terms of the scattering angle Θ. In this equation, $q(\Theta)$ is the multi-scattering contribution, that is simulated by the Reduced Multiple Scattering algorithm (REDM), an optimized radiative transfer code developed by Nakajima et al. (1983) for a plane parallel atmosphere. Moreover, the relationship between the total air ensemble of the particulate and molecular aerosol optical depths is given by:

$$\delta = \delta_a + \delta_m \quad (3)$$

From Equations (1) and (2), the ratio $R(\Theta)$ can be defined and written as:

$$R(\Theta) = \frac{E(\Theta)}{Fm_0} = \omega\delta P(\Theta) + q(\Theta) = \beta(\Theta) + q(\Theta) \quad (4)$$

In Equation (4), $\beta(\Theta)$ has been defined as the total scattering coefficient, which includes both molecular and aerosol scattering. The algorithm iteratively extracts the multiple scattering term $q(\Theta)$ from the data $R(\Theta)$ to retrieve $\beta(\Theta)$. In each of these steps, the algorithm retrieves the aerosol size distribution $v(r)$ by inversion of $\beta(\Theta)$ and $\delta(\lambda)$. In turn, this new $v(r)$ is fed into the RTM for estimating a new ratio $R'(\Theta)$, and is compared with the experimental ratio $R(\Theta)$ to evaluate the mean squared difference $\varepsilon(R)$. The iterative process is stopped when this deviation is less than 10% (solution accepted), or the maximum 10 iterations are exceeded (solution rejected).

Cloud screening filters based on lateral symmetry (such as the method used by AERONET) cannot be applied to this PREDE

database, because only one side of the solar almucantar plane was measured. Auxiliary instruments (such as all sky imagers, pyranometers or pyrgeometers) are not available at the site, preventing the application of other elaborated cloud screening methodologies. Therefore, the automatic acceptance/rejection of diffuse data is implicitly performed by the application of the previous convergence threshold $\varepsilon(R)$ between experimental and retrieved data. When the sky is not cloud free, the deviation between experimental and retrieved radiance is high and the iteration is stopped. Specific situations with thin and homogeneous cirrus clouds cannot be discarded with this method. However, these cases are difficult to identify with the other methods too.

3.2. Air mass characterization

In this study the Hybrid Single-Particle Lagrangian Integrated Trajectory Model (HYSPLIT; February 2009 version) developed by NOAA (Draxler and Rolph, 2009) was used to determine the origin of air masses affecting Plymouth. The HYSPLIT trajectories are computed as those ending at three different levels over the Plymouth site. These levels were 500, 1500 and 3000 m asl. The HYSPLIT simulations were run for a flight time of 120 h (Estellés et al., 2007). A 3D model of vertical velocity (Draxler, 1996) was used and the National Centre for Environmental Prediction/National Centre for Atmospheric Research (NCEP/NCAR) reanalysis database chosen for the meteorological field input data. Using this configuration the back trajectories finishing at 1200 GMT over Plymouth for each day containing aerosol data were computed.

Specific source/path regions were defined following meteorological definitions from the UK Met Office. These classes are shown in Fig. 2. Class Am is Arctic maritime, carrying predominantly maritime aerosols, with a low contribution of rural or anthropogenic aerosols. Pm is Polar maritime: typically it is a north-westerly airstream, originating over northern Canada and Greenland and characterized by low loadings of maritime aerosols. Tm is Tropical maritime: this is a southwesterly airstream coming from the Azores region. This type is very infrequent in the analyses presented in this study. It is likely to contain maritime aerosols associated with high water vapor content. rPm is returning Pm air mass but here it is more frequently represented as a transition type between the Pm and Tm. Tc is defined as a Tropical continental air mass originating over northern Africa, and has the potential to carry Saharan mineral dust. However most of the coarse mode aerosol content could have been deposited on transit to the UK. A certain amount of anthropogenic aerosols could also be carried from Western Europe. Finally, classes Ac and Pc are subtypes of the Polar continental air mass and have been defined separately to identify any differences in the degree of anthropogenic urban and industrial aerosol loading from Europe. In general, the Pc class should be affected by urban and industrial pollution, and rural aerosols.

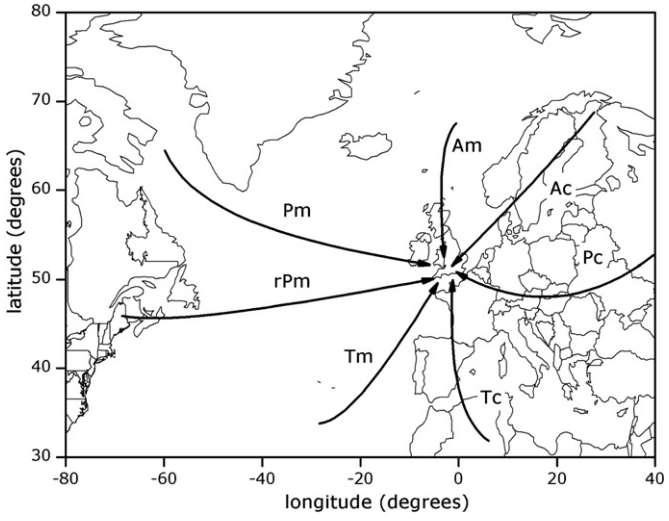

Fig. 2. Sectors defined for the air mass classification: Am (Arctic maritime), Ac (Arctic continental), Pc (Polar continental), Tc (Tropical continental), Tm (Tropical maritime), rPm (returning Polar maritime) and Pm (Polar maritime).

The categorization of the computed daily back trajectories was carried out by visual inspection. Only cases that were consistently classified for the three levels have been considered, representing 48% of the total 314 cases.

4. Results

4.1. Temporal evolution

4.1.1. Aerosol optical depth (AOD)

Fig. 3a shows the annual evolution of the daily averaged AOD at 500 nm over the eight years of measurements performed in Plymouth. A total of 314 daily averages are available implying less than 10% of total days have been successfully measured or inverted. Weather in Plymouth is highly variable with frequent low, thick clouds and occasional mists preventing optical aerosol retrievals. Many of these 314 days have a poor time resolution due to cloud evolution. However the high frequency of radiance measurements (every 10 min) employed at the site maximized the chances of finding cloudless intervals and successful retrievals. Days with less than 2 valid hourly means are rejected in this seasonal analysis; the hourly averages are also rejected if they do not contain more than two instantaneous measurements.

Analysis of the 500 nm channel has been chosen because it is widely quoted in sun photometric and remote sensing applications, and is generally representative of visible band wavelengths. In spite of the low number of daily measurements in Fig. 3a the variability of aerosol events can clearly be seen, with a relatively smooth annual cycle displayed in comparison to continental sites. Aerosol loadings tend to be reduced in winter (December, January and February), but there is little to separate the spring (March, April and May), summer (June, July and August) and autumn (September, October and November). This is shown clearly in Fig. 3b. The annual mean and median AOD at 500 nm were 0.18 and 0.19, with a mean standard deviation of 0.08. Some of the high outliers are possibly caused by cirrostratus or mists whose influence could not be completely discarded. But the data spread throughout the year is caused by the high day-to-day atmospheric variability typical of the coastal mid-latitudes, as opposed to remote oceanic areas that are characterized by a more stable atmospheric situation (Smirnov et al., 2002).

It is interesting to highlight the particular high AOD found during March and August 2003. During mid March 2003, a pollution event was recorded from the UK urban air monitoring network (Kent, 2003) and was mainly related to eastern European air masses. During the first half of August 2003, Western Europe suffered a severe and persistent heat wave related to the arrival of an air mass originating over North Africa (Lyamani et al., 2006). This air mass was responsible of the arrival of fine particles from the numerous forest fires that occurred in south-western Europe and perhaps also brought mineral dust from the Sahara. This event occasioned the extreme maxima found in Fig. 3.

Fig. 3b shows generally higher AOD in the spring and summer months. The spring and summer months are characterized by more intense solar heating: this has the effect of deepening the boundary

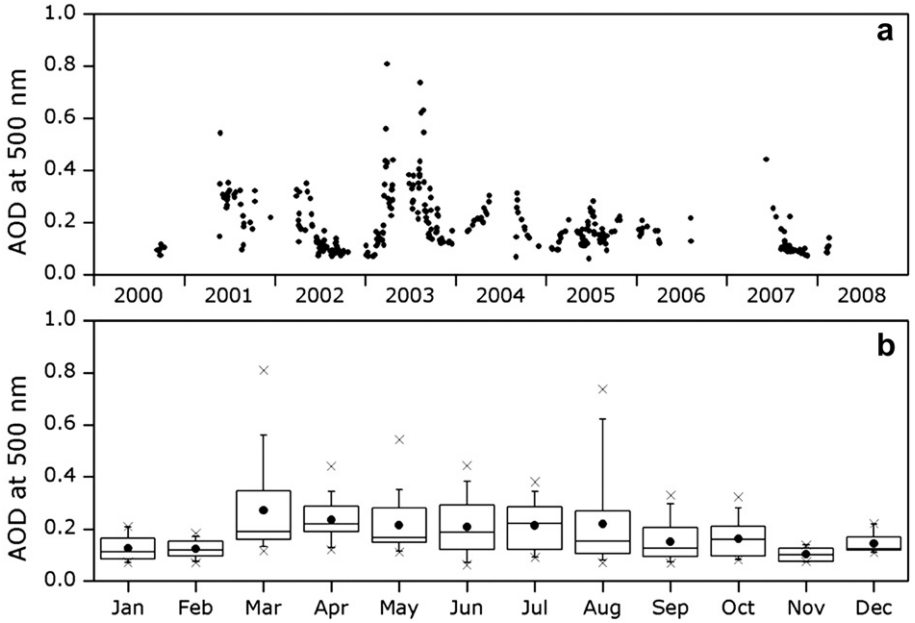

Fig. 3. AOD at 500 nm: (a) daily means along the whole database, (b) box chart for monthly statistics. In the box charts, the solid dot represents the monthly mean. The box is determined by the 25th and 75th percentiles, and the whiskers are determined by the 5th and the 95th percentiles. Crosses indicate the 1st and 99th percentiles. The median is represented by the divisor line of the box.

layer (effectively increasing the aerosol pathlength) and also introducing more aerosol particles into the lower atmosphere by increasing the turbulence. Anticyclonic conditions also have the effect of increasing aerosol content in the atmosphere by effectively trapping them in the lowest layers and enhancing stagnation; the lack of effective precipitation also means that the atmosphere is not cleansed. Moreover, an increase of AOD during warmer months is expected not only by local emission and transformation processes but by advection from remote sources such as continental Europe or North Africa (Estellés et al., 2007). Similar seasonal patterns were also present for Bermuda (Smirnov et al., 2002) a subtropical site in the North Atlantic Ocean (32°22′N). This site was considered to be not truly maritime all the time, due to influence of anthropogenic aerosols from North America and mineral dust from the Sahara.

4.1.2. Ångström wavelength exponent (α)

Fig. 4a shows the time-series of the daily mean α: an annual pattern is more strongly apparent than for AOD (Fig. 3), with increasing values in late summer months (Fig. 4b) and lower values in autumn and winter months (this pattern is very clear in 2005).

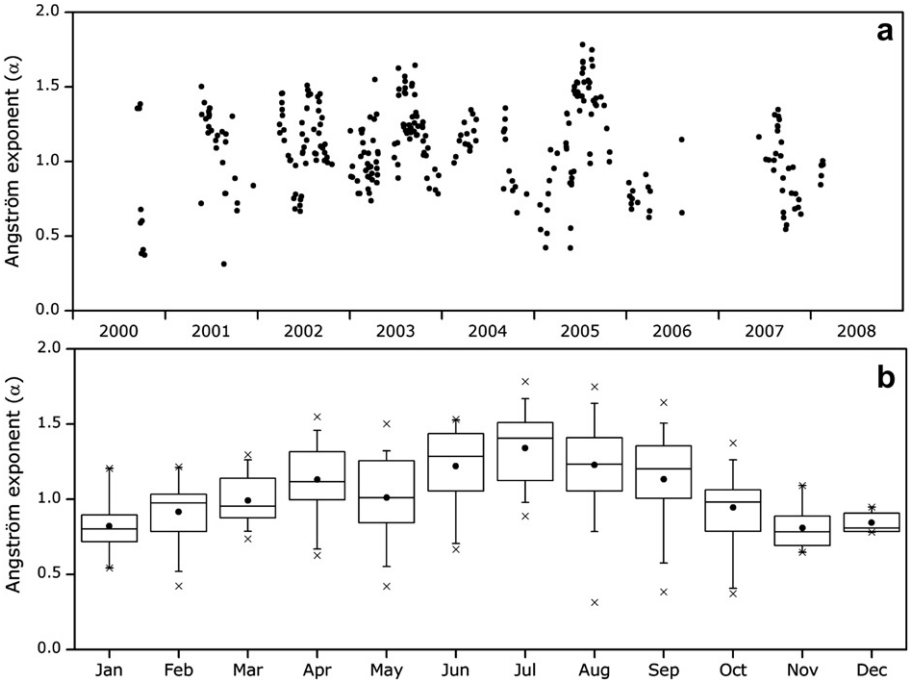

Fig. 4. Ångström Exponent: (a) daily means along the whole database, (b) box chart for monthly statistics. As Fig. 3 for explanation of symbols in (b).

The mean annual α is 1.03 ± 0.21 (median 1.00). It is probable that marine aerosols are responsible for the average annual value and some of the annual pattern we have found. The absence of strong anthropogenic and desert aerosol sources in close proximity to Plymouth makes this hypothesis plausible.

The AOD and α exponent are related: the higher summer turbidities are frequently related to the higher exponent means (slightly finer particles), the reverse being true in winter with coarser particles dominating. The finer summer time aerosols are related to the presence of air masses affected by anthropogenic particles. During the summer the cleansing action of precipitation, removing these aerosols from the atmosphere, may be less frequent or even effective. Humidity and water vapor columnar content can affect the relative size of the aerosols through hygroscopic phenomena, mainly in winter months.

4.1.3. Aerosol volume distributions (v(r))

Fig. 5 shows the seasonally averaged aerosol size distributions ($v(r) = dV/d\ln r$) for winter (DJF), spring (MAM), summer (JJA) and autumn (SON). The dots represent the experimental points and the lines a fit to a bimodal distribution:

$$\frac{dV}{d\ln r} = \sum_{i=1,2} \frac{V_i}{\sqrt{2\pi}\ln\sigma_i} \exp\left[-\frac{1}{2}\left(\frac{\ln(r/r_i)}{\ln\sigma_i}\right)^2 \right] \quad (5)$$

where subscripts i = 1,2 refer to the fine and coarse modes respectively; V the modal volume; σ the size bin width and; r the aerosol radius. The R^2 value for the fit to Equation (5) is always greater than 0.95.

Fig. 5 shows that the spring distribution has the highest fine (0.019 $\mu m^3\ \mu m^{-2}$) and coarse modes (0.023 $\mu m^3\ \mu m^{-2}$) with both modes having similar volumes. A similar fine mode (0.018 $\mu m^3\ \mu m^{-2}$) is found in the summer, consistent with the summer values of the Ångström exponent. This behavior is closely related to the AOD and wavelength exponent (Figs. 3 and 4) and could be easily explained by the presence of a stronger load of anthropogenic and fine aerosols in the atmosphere.

In contrast winter shows the lowest modes (0.0095 and 0.014 $\mu m^3\ \mu m^{-2}$), consistent with the minimum AOD. Although the fine mode is similar for both autumn and winter distributions, the modal volume and radius for the coarse mode is much larger in autumn, almost as high as in spring.

Finally, it is worth noting that in winter, the coarse mode makes the dominant contribution to the total aerosol load. It has a comparable modal volume as the summer case. This is likely related to the generally low aerosol burden, with low variability found at Plymouth, but dominated by larger marine aerosols.

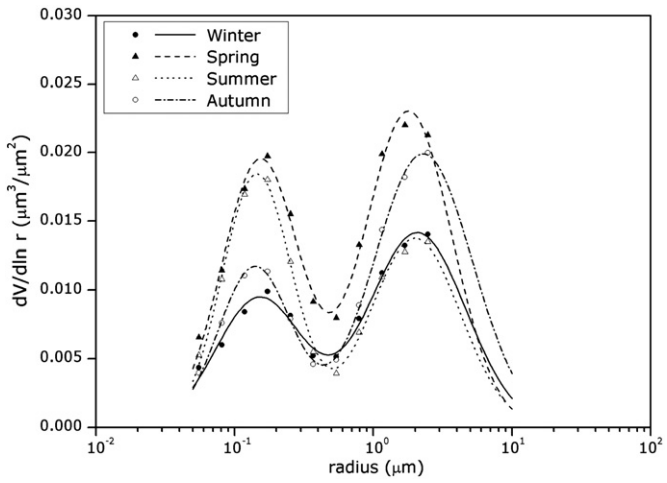

Fig. 5. Seasonally averaged volume distributions. Dots correspond to inverted data; lines are bimodal fits to Equation (5).

4.1.4. Refractive index (RRI and IRI) and single scattering albedo (SSA)

The uncertainty of the refractive index and single scattering albedo retrieval is generally high, with the highest uncertainties occurring when the aerosol burden is low. Kim et al. (2004) performed a sensitivity analysis and found that the difference between simulated and retrieved values of SSA was as high as 0.08 for low aerosol optical depths and zenith angles (0.2 and 30° respectively). Therefore, our retrievals must be taken with extreme care as the PML dataset is dominated by low AOD.

The real refractive index (RRI) shows a yearly mean value of 1.46, with an annual pattern with minimum values in summer (June and July, mean value of 1.42) and maximum values in winter. The imaginary refractive index (IRI) varies in the range −0.01 to 0.00, with an annual mean of −0.002. These are very low values and indicative of non-absorbing aerosols, expected in regions largely free from anthropogenic influence.

The SSA is an important parameter influencing the aerosol radiative forcing in the atmosphere (Dubovik et al., 2002) and it is related to the absorption properties of the aerosols. Fig. 6a and b show the daily averages for the SSA in the visible band. The yearly mean SSA is 0.97 (median 0.98) with a standard deviation of about 0.01, lower than the inherent uncertainty (higher than 0.05 for AOD lower than 0.2 (Dubovik et al., 2002)). These high values of SSA are related to non-absorbing aerosols, and are consistent with main sea–salt aerosols or possibly hygroscopic particles covered by a thin layer of water. The main pattern is for lower values in the summer months and beginning of spring months. These low values could be related to episodic intrusions of darker aerosols of a more anthropogenic origin.

Comparing with values published in the literature, Smirnov et al. (2003) found a refractive index of about 1.37–0.001i, and a SSA around 0.98 for the maritime aerosol model. In spite of the high uncertainty and using different inversion algorithms, our absorption estimates (0.97 for maritime air masses) are quite comparable. In relation to the real part of the refractive index, our retrievals result in a higher annual mean (1.46).

4.2. Air mass origin influence

4.2.1. Classification of aerosol properties

Fig. 7 shows the AOD and Ångström exponent classification in terms of back trajectories. There is a distinct air mass dependency on AOD with the maritime classes giving similar (low) values of 0.13–0.15, and the continental types giving the highest (0.14–0.34) consistent with a stronger source of terrestrial and anthropogenic particles.

The maximum air-mass classified AOD (mean 0.34, median 0.30) is reached for Tc. Air masses coming from southern Europe are the most turbid with particles originating from the drier soils of southern Europe and N. Africa; Saharan desert dust or particles originating in summer forest fires cannot be discounted. This air mass is most common during summer (June, July and August) and is caused by a high pressure system over northern or eastern Europe. This air-mass may be associated with high temperatures such as the 2003 summer heat wave which was associated with maximum aerosol concentration (Lyamani et al., 2006). During winter such air masses are more stable and may be associated with persistent cloudiness, preventing sun photometric measurements.

Continental air masses Pc and Ac show much lower AOD values than the Tc case even for the highest percentiles (U75, U95 and

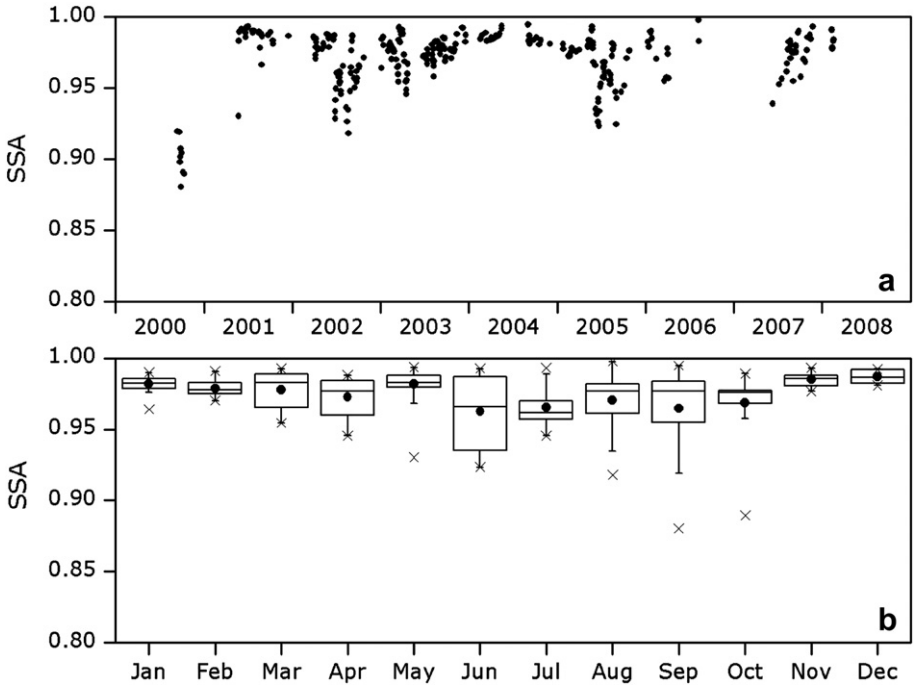

Fig. 6. Single scattering albedo: (a) daily means along the whole database, (b) box chart for monthly statistics. As Fig. 3 for explanation of symbols in (b).

U99). The central European (Pc) air masses have slightly higher AOD values than the Scandinavian (Ac) cases with a mean of 0.20 and 0.14 respectively, possibly due to differing degrees of anthropogenic activity. There is no such difference between the three northern Atlantic maritime air masses.

Fig. 7 also shows an analysis of the Ångström exponent. The three main northern Atlantic classes (Am–Pm–rPm) again have almost the same behavior with an exponent of between 0.96 and 1.03. The European Pc and Ac classes have slightly higher exponents, possibly related to finer anthropogenic aerosols in the size distribution. However these values are not particularly high (means and medians around 1.10–1.20, U95 about 1.50) indicating a relatively weak influence of remote pollution sources. Annual mean values in Plymouth are more similar to results from the maritime air masses than the continental ones, emphasizing the strong maritime influence. In contrast, the lowest exponent is reached for the Tc air masses (mean 0.83) indicative of coarser particles brought from drier continental soils or even the Sahara.

Smirnov et al. (2003) proposed a maritime aerosol model based on AERONET data for three different island sites located in the

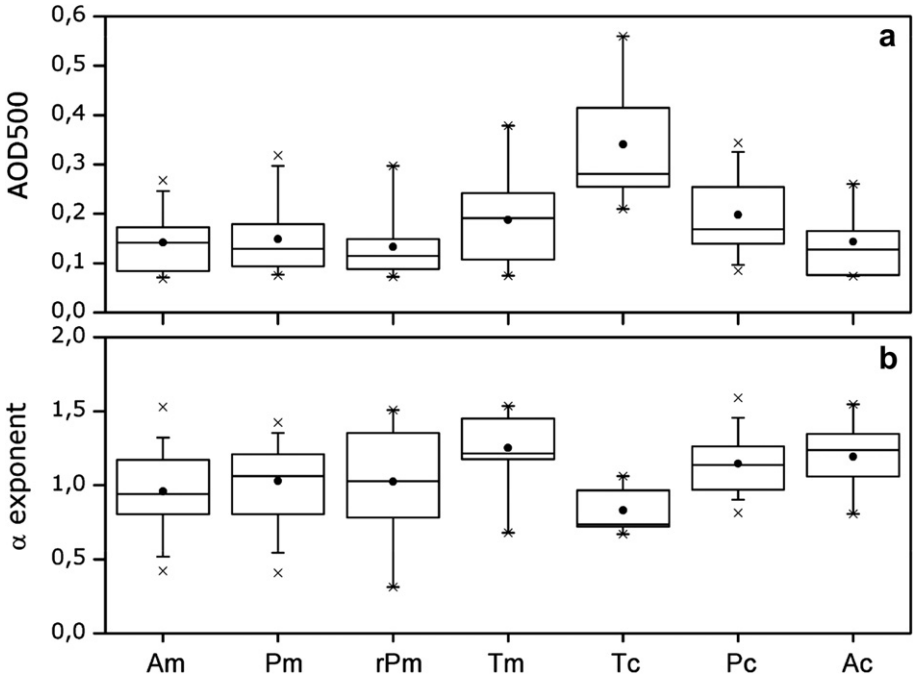

Fig. 7. Classification of daily means of (a) AOD at 500 nm and (b) α exponent in terms of the pure air masses.

subtropical North Atlantic Ocean. To develop this aerosol model only data with AOD < 0.15 and α < 1.0 were used. The mean values obtained for marine air masses at Plymouth are below these maximum thresholds.

In a previous compilation performed by Smirnov et al. (2002), a study of other oceanic sites including Bermuda was performed. In their study, the mean AOD at 500 nm found in the Atlantic site was 0.14, in close agreement with our findings for the three northern maritime air masses (0.13–0.15). On the other hand, the peak frequency of α in Bermuda was found to be 0.9, with a distribution skewed towards higher α. This is also consistent with our results ranging between 0.96 and 1.03. Therefore, AOD and α in Plymouth are higher than the Bermuda site due in part to the slight influence from continental and anthropogenic sources.

Fig. 8 shows the daily volume distributions classified in terms of the seven air mass types. The three main north Atlantic classes have a similar minimum fine mode as no important urban or industrial sources are expected. The modal fine radius and volume concentration range from 0.11 to 0.12 μm, and 0.011 to 0.013 $\mu m^3\ \mu m^{-2}$ respectively. Smirnov et al. (2002) found a slightly higher fine modal radius (0.14 μm) for Bermuda islands, with a modal volume of 0.024 $\mu m^3\ \mu m^{-2}$. This fine mode values are more comparable to the Tm southern air mass class (0.17 μm and 0.024 $\mu m^3\ \mu m^{-2}$). The higher radius is possibly related to an increase in water vapor content (dependent on latitude) that affects hygroscopic aerosols.

Good agreement is also achieved for the maritime coarse mode: our results are 2.3–2.8 μm, and 0.026–0.054 $\mu m^3\ \mu m^{-2}$ for coarse modal radius and volume respectively. Correspondingly, Smirnov et al. (2002) values were 2.55 μm and 0.041 $\mu m^3\ \mu m^{-2}$. Our results exhibit slightly different coarse modes for the maritime air masses, the higher the latitude of the source, the lower the coarse mode is.

In contrast the Tc class has a much larger coarse mode ($Vc = 0.125\ \mu m^3\ \mu m^{-2}$) which drives the higher AOD and the lower Ångström exponent, although the modal radius is somewhat smaller ($Rc = 1.8$ μm). This could possibly be related to mineral dust or continental aerosol influence from the south. The coarser particles are removed faster than the fine particles: a comparison with sites directly to the south could possibly elucidate a change in the modal radius. The modal volume is comparable to values found for places more influenced by direct dust intrusions (Dubovik et al., 2002) and thus an interference of other causes (such as cirrus cloud contamination) cannot be disregarded.

The Tc and Pc fine mode is quite similar. It is not clear however if this is due to the same type of aerosol. The Pc class is most probably composed of anthropogenic industrial or urban aerosols. The Tc class could also be influenced by a fine mineral mode.

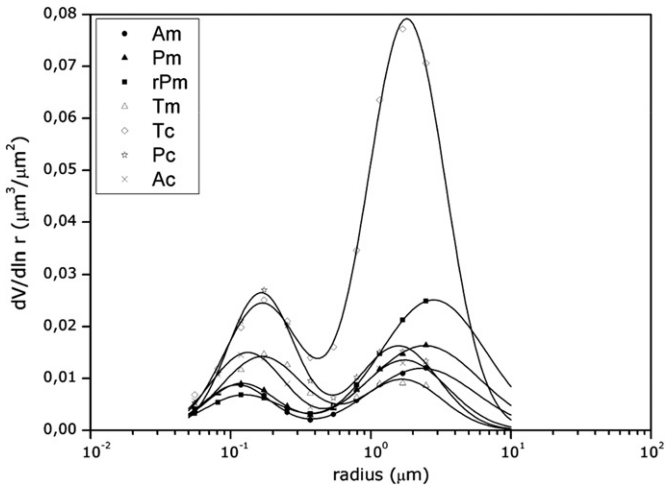

Fig. 8. Averaged aerosol volume distributions in terms of the air mass class.

5. Conclusions

A multiyear calibration, based on the improved Langley plot method (SKYIL), has been used for the processing of the eight year PML sun/sky photometric dataset. Although cloudy skies are frequent along the western English Channel coast, such a long dataset has allowed a thorough statistical characterization of the column integrated aerosol optical properties for this site.

The results show that the aerosol optical depth is generally mid-low throughout the year, with an AOD at 500 nm of 0.18 ± 0.08. The Ångström wavelength exponent has an annual mean of 1.03 ± 0.21 with U95 of 1.53, indicative of a region only weakly affected by local or remote anthropogenic pollution. On the other hand, the annual percentile U5 of AOD is about 0.08, slightly higher than continental sites where low atmospheric moisture leads to very clear skies.

The AOD seasonal variation is not strong and the maximum period is smooth and well distributed along a plateau extending from March to October. The Ångström exponent and volume distributions shows also a size dependent annual pattern with higher values during the summer months, perhaps more affected by anthropogenic sources from continental Europe, given the absorption indexes retrieved here. The coarse mode is dominant for all the seasons except summer, when the fine mode dominates.

Atlantic air masses clearly dominate and are characterized by low AOD and the presence of coarser, possibly sea-salt, aerosols. Episodic influence of European polluted air masses is also apparent, although these are generally weak (mean AOD and wavelength exponent of 0.20 and 1.15, respectively), and when averaged over the year their influence on the climatology is weakened. The spring–summer higher turbidities are possibly driven by transport from far southern Europe regions. Lack of precipitation, dryness of the continental surface, strong air turbulence in the boundary layer and atmospheric stability coupled with anthropogenic inputs are key to understanding the higher turbidity of tropical continental air masses, with an AOD and wavelength exponent of 0.34 and 0.83 respectively, constituting the maximum and minimum of the classification.

Acknowledgments

V. Estellés thanks the Ministerio de Ciencia e Innovación (Spain) for the current fellowship under the *Juan de la Cierva* programme (JCI-2009-04455) and the postdoctoral fellowship (program POSTDEXT, reference 2008-0262). T.J. Smyth was supported by the NERC Oceans 2025 Theme 10 (Sustained Observations) and the NERC APPRAISE project. Solar radiation group at University of Valencia was funded with projects CGL2009-07790 from the Ministry of Science and Innovation (MICINN) and PROMETEO-2010-064 from the Valencian Autonomous Government.

Reference

Boi, P., Tonna, G., Dalu, G., Nakajima, T., Olivieri, B., Pompei, A., Campanelli, M., Rao, R., 1999. Calibration and data elaboration procedure for sky irradiance measurements. Applied Optics 38, 896–907.

Campanelli, M., Nakajima, T., Olivieri, B., 2004. Determination of the solar calibration constant for a sun–sky radiometer: proposal of an in situ procedure. Applied Optics 43, 651–659.

Campanelli, M., Estellés, V., Tomasi, C., Nakajima, T., Malvestuto, V., Martínez-Lozano, J.A., 2007. Application of the SKYRAD Improved Langley plot method for the in situ calibration of CIMEL Sun–sky photometers. Applied Optics 46, 2688–2702.

Campanelli, M., Estellés, V., Smyth, T., Tomasi, C., Martínez-Lozano, J.A., Claxton, B., Muller, P., Pappalardo, G., Pietruczuk, A., Shanklin, J., Colwell, S., Wrench, C., Lupi, A., Mazzola, M., Lanconelli, C., Vitale, V., Congeduti, F., Dionisi, D.,

Cardillo, F., Cacciani, M., Casasanta, G., Nakajima, T., 2012. Monitoring of Eyjafjallajökull volcanic aerosol by the new European Skynet Radiometers (ESR) network. Atmospheric Environment 48, 33–45. http://dx.doi.org/10.1016/j.atmosenv.2011.09.070.

Cruz, C.N., Pandis, S.N., 1997. A study of the ability of pure secondary organic aerosol to act as cloud condensation nuclei. Atmospheric Environment 31, 2205–2214.

Draxler, R.R., 1996. Boundary layer isentropic and kinematic trajectories during the August 1993 North Atlantic Regional Experiment Intensive. Journal of Geophysical Research 101, 29255–29268.

Draxler, R.R., Rolph, G.D., 2009. HYSPLIT (Hybrid Single – Particle Lagrangian Integrated Trajectory). Available at:. Air Resour. Lab., Natl. Oceanic Atmos. Admin, Silver Spring, Md (last access on March 2011). http://www.arl.noaa.gov/ready/hysplit4.html.

Dubovik, O., Holben, B.N., Eck, T.F., Smirnov, A., Kaufman, Y.K., King, M.D., Tanré, D., Slutsker, I., 2002. Variability of absorption and optical properties of key aerosol types observed in worldwide locations. Journal of Atmospheric Science 59, 590–608.

Estellés, V., Martínez-Lozano, J.A., Utrillas, M.P., 2007. Influence of air mass history on the columnar aerosol properties at Valencia, Spain. Journal of Geophysical Research 112. http://dx.doi.org/10.1029/2007JD008593.

Estellés, V., Campanelli, M., Utrillas, M.P., Expósito, F.J., Martínez-Lozano, J.A., 2012. Comparison of AERONET and SKYRAD4.2 inversion products retrieved from a Cimel CE318 sunphotometer. Atmospheric Measurement Techniques 5, 569–579. http://dx.doi.org/10.5194/amt-5-569-2012.

Haywood, J., Schulz, M., 2007. Causes of the reduction in uncertainty in the anthropogenic radiative forcing of climate between IPCC (2001) and IPCC (2007). Geophysical Research Letters 34, L20701. http://dx.doi.org/10.1029/2007GL030749.

Hoerling, M., Kumar, A., Eischeid, J., Jha, B., 2008. What is causing the variability in global mean land temperature? Geophysical Research Letters 35, L23712. http://dx.doi.org/10.1029/2008GL035984.

Holben, B.N., Eck, T.F., Slutsker, I., Buis, J.P., Setzer, A., Vermote, E., Reagan, J.A., Kaufman, Y., Nakajima, T., Lavenu, L., Jankowiak, I., Smirnov, A., 1998. AERONET – a federated instrument network and data archive for aerosol characterization. Remote Sensing of Environment 66, 1–16.

Intergovernmental Panel on Climate Change (IPCC), 2007. Climate change 2007: the physical Science Basis. In: Solomon, S., Qin, D., Manning, M., Chen, Z., Marquis, M., Averyt, K.B., Tignor, M., Miller, H.L. (Eds.), Contribution of Working Group I to the Fourth Assessment Report of the Intergovernmental Panel on Climate Change. Cambridge University Press, Cambridge, United Kingdom and New York, NY, USA, p. 996.

Kent, A., 2003. Air Pollution Forecasting: Pollution Episode Report (March and April 2003). Available at: http://uk-air.defra.gov.uk/reports/cat12/ad-hoc_pm10_report_febmar03_episode.pdf.

Kim, D.H., Sohn, B.J., Nakajima, T., Takamura, T., Takemura, T., Choi, B.C., Yoon, S.C., 2004. Aerosol optical properties over East Asia determined from ground-based sky radiation measurements. Journal of Geophysical Research 109, D02209. http://dx.doi.org/10.1029/2003JD003387.

Lyamani, H., Olmo, F.J., Alcántara, A., Alados-Arboledas, L., 2006. Atmospheric aerosols during the 2003 heat wave in southeastern Spain I: spectral optical depth. Atmospheric Environment 40, 6453–6464. http://dx.doi.org/10.1016/j.atmosenv.2006.04.048.

Nakajima, T., Tanaka, M., Yamauchi, T., 1983. Retrieval of the optical properties of aerosols from the aureole and extinction data. Applied Optics 22, 2951–2959.

Nakajima, T., Tonna, G., Rao, R., Boi, P., Kaufman, Y., Holben, B.N., 1996. Use of sky brightness measurements from ground for remote sensing of particulate polydispersions. Applied Optics 35, 2672–2686.

Shaw, G.E., 1976. Error analysis of multi-wavelength sun photometry. Pure and Applied Geophysics 114, 1–14.

Smirnov, A., Holben, B.N., Kaufman, Y.J., Dubovik, O., Eck, T.F., Slutsker, I., Pietras, C., Halthore, R.N., 2002. Optical properties of atmospheric aerosol in maritime environments. Journal of Atmospheric Science 59, 501–523.

Smirnov, A., Holben, B.N., Dubovik, O., Frouin, R., Eck, T.F., Slutsker, I., 2003. Maritime component in aerosol optical models derived from Aerosol Robotic Network data. Journal of Geophysical Research 108, D1. http://dx.doi.org/10.1029/2002JD002701.

Smirnov, A., , et al.45 authors, 2011. Maritime aerosol network as a component of AERONET – First results and comparison with global aerosol models and satellite retrievals. Atmospheric Measurement Techniques 4, 583–597.

Takamura, T., Nakajima, T., SKYNET Community Group, 2004. Overview of SKYNET and its activities. Óptica Pura y Aplicada 37, 3303.

Zhang, R., Delworth, T.L., Held, I.M., 2007. Can the Atlantic Ocean drive the observed multidecadal variability in Northern Hemisphere mean temperature? Geophysical Research Letters 34, L02709. http://dx.doi.org/10.1029/2006GL028683.